# Graphene quantum dot-based magnetic relaxation switch involving magnetic separation for enhanced performances of endoglin detection using ultra-low-field nuclear magnetic resonance relaxometry

*Yongqiang Li* [a, e, h, 1], *Zhifeng Shi* [b, d, f, g, 1], *Liuyang Shang* [a, e, h], *Quan Tao* [a, e, h], *Qisheng Tang* [b, d, f, g], *Hans-Joachim Krause* [c, h], *Siwei Yang* [a, e, *], *Guqiao Ding* [a, e, *], and *Hui Dong* [a, e, h, *]

[a] Shanghai Institute of Microsystem and Information Technology (SIMIT), Chinese Academy of Sciences (CAS), Shanghai 200050, P. R. China.
[b] Department of Neurosurgery, Huashan Hospital, Shanghai Medical College, Fudan University, Shanghai, P. R. China.
[c] Institute of Biological Information Processing (IBI-3), Forschungszentrum Jülich (FZJ), D-52425 Jülich, Germany.
[d] National Center for Neurological Disorders, Shanghai, P. R. China.
[e] Center of Materials Science and Optoelectronics Engineering, University of Chinese Academy of Sciences (UCAS), Beijing 100049, P. R. China.
[f] Shanghai Key Laboratory of Brain Function Restoration and Neural Regeneration, Shanghai, P. R. China.
[g] Neurosurgical Institute of Fudan University, Shanghai, P. R. China.
[h] Joint Research Institute on Functional Materials and Electronics, Collaboration between SIMIT and FZJ.
[1] These authors contributed equally to this work.
[*] Corresponding authors: Siwei Yang – E-mail: yangsiwei@mail.sim.ac.cn; Guqiao Ding – E-mail: gqding@mail.sim.ac.cn; Hui Dong – E-mail: donghui@mail.sim.ac.cn

ABSTRACT

Magnetic relaxation switches (MRS) based on target-induced state changes of magnetic nanoparticles are vital approaches for biomolecule detection in *in vitro* diagnosis. Recently, magnetic graphene quantum dots have been employed as magnetic probes instead of iron oxide nanoparticles and showed high sensitivity. Introducing magnetic separation into an MRS assay before the relaxometry measurements can enhance the sensitivity, elevate accuracy, and expand the linear region. In this work, magnetic separation-assisted MRS was developed to detect endoglin utilizing iron oxide as the magnetic carrier and magnetic graphene quantum dots as the magnetic probe. The assay possesses a broad linear region from 5 ng/mL to 50 μg/mL and a sensitive limit of detection of 1.3 ng/mL, which is two orders of magnitude lower than that of MRS without magnetic separation. The high accuracy and consistency have been proved for endoglin (CD105) detection in real samples. This graphene quantum dot-based MRS involving magnetic separation provides a new route for enhancing the sensitivity and accuracy of biomolecule detection.

KEYWORDS: magnetic separation, magnetic relaxation switch, graphene quantum dots, ultra-low-field NMR, CD105

## 1. Introduction

Magnetic nanoparticles in the dispersed or aggregated state usually lead to differences in heterogeneous local magnetic fields, which are generally reflected as a change of relaxation time ($T_1$ or $T_2$) recorded by nuclear magnetic resonance (NMR) relaxometry [1, 2]. This phenomenon can be utilized to realize conventional magnetic relaxation switches (MRS) in sensing biological targets like viruses [3, 4], proteins [5-8], cancer cells [9-11], bacteria [12-14], and liposomes [15]. The key of quantitative MRS is to have highly monodisperse magnetic nanoparticles of a consistent size that result in precise and quantitative changes in relaxation time when cleaved or aggregated [16]. Because of its biocompatibility, $Fe_3O_4$ is generally employed as the MRS probe to convert the bio-interactions into a magnetic signal change [4, 7, 15-18]. To ensure the high dispersity of $Fe_3O_4$ and protect the magnetic cores from any changes driven by the surrounding media, surface coatings on $Fe_3O_4$ are universally used [16], which can also provide ligands to bind the aptamers for specific sensing. Nevertheless, surface coatings require laborious preparation.

Although great achievements of MRS involving $Fe_3O_4$ have been attained, some carbon-based magnetic nanomaterials also reveal a high potential in MRS due to their superior properties. Since graphene quantum dots (GQDs) were first reported in 2004 [19], their modifiable structures, tunable properties [20], high water dispersibility, and excellent biocompatibility make them well suited for biological applications [21-23]. By combining GQDs and paramagnetic $Gd^{3+}$, the obtained magnetic GQDs exhibit high magnetic relaxivity that is mainly contributed by the tunable microenvironment of GQDs. Additionally, the abundant groups of GQDs can directly serve as binding sites for aptamers. Recently, magnetic GQDs have been applied in the detection of biomolecules with high sensitivity due to their high relaxivities [24, 25].

However, MRS assays based on target-induced aggregation or disaggregation of magnetic nanoparticles have some shortcomings. MRS usually depends on antibody-antigen recognition, but the state of magnetic nanoparticles remains unchanged, resulting in the loss of sensitivity [2, 26]. High concentrations of magnetic nanoparticles may also impair stability and linear detection range, so that sensitivity and accuracy will be sacrificed [27]. To circumvent these limitations, magnetic separation can be introduced to MRS, in which magnetic nanoparticles have two roles: they serve as i) magnetic carriers for separation and ii) magnetic probes for signaling. MRS involving magnetic separation is usually advantageous in enhancing sensitivity [28, 29].

In this work, a magnetic separation-assisted MRS (MS-MRS) composed of $Fe_3O_4$ (100 nm) as the magnetic carrier and magnetic GQDs as the magnetic probe was developed. As a reference, magnetic GQDs independently served as the probe to construct a conventional MRS without magnetic separation (denoted as G-MRS). Both the MRS assays were used to detect endoglin (CD105), which is a homodimeric transmembrane protein mainly distributed in the extracellular region and plays a crucial role in angiogenesis [30]. The CD105 is often expressed at a much higher level (20–2000 folds increase) in tumor tissues than in healthy tissues because the proliferation of endothelial cells is vigorous [31]. Hence, CD105 can be used as a biomarker for the general determination of tumors. In the MS-MRS assay, both the magnetic carrier and probe can specifically bind to CD105 at different sites. After that, a magnet was used to remove the particles bonded to the magnetic carrier and the magnetic probe was thus left. Using the homemade ultra-low field (ULF) NMR relaxometry, the relaxation times of the samples can be measured. The MS-MRS exhibits high sensitivity, a remarkable linear region, and more distinguishable relaxation times compared with those of G-MRS. Additionally, MS-MRS can be used to detect CD105 in human serum with high accuracy and consistency.

## 2. Materials and methods

### *2.1. Materials*

The GQDs powder was purchased from CASYUEDA Materials Technology Co., Ltd. (Shanghai, China) and used as received. Hexaethylene glycol ($PEG_6$, 97.0%), $Gd(NO_3)_3$•$6H_2O$ (99.9%), bovine serum albumin (BSA), phosphate buffer saline (PBS) buffer (pH = 6.0 and 7.2), and tris(hydroxymethyl)aminomethane (Tris) buffer (pH = 8.0) were purchased from Aladdin Co., Ltd. (Shanghai, China) and used without further purification. Carboxylated ferroferric oxide ($Fe_3O_4$) that dispersed in deionized water was purchased from Nanjing Nanoeast Biotech Co., Ltd. (Nanjing, China) and used as received. 1-Ethyl-3-(3-dimethylaminopropyl) carbodiimide (EDC), N-hydroxysuccinimide (NHS), and Tween® 20 were purchased from Sinopharm Chemical Reagent Co., Ltd. (Shanghai, China) and stored in accordance with the manual. The CD105 protein (Cat.# 10149-H08H), CD105 antibody for capture (Cat.# 10149-MM11, $Ab_1$), CD105 antibody for detection (Cat.# 10149-MM05, $Ab_2$), and Anti-G protein alpha S/GNAS Antibody (Cat.# 100828-T36) were purchased from Sino Biological Inc. (Beijing, China). CD105 Enzyme-linked immunosorbent assay (ELISA) kit (Cat.# KIT10149) was purchased from Sino Biological Inc. (Beijing, China) and used according to the manufacturer's protocol. Deionized water (resistivity ~18.2 MΩ cm at 25 °C) was obtained using a Milli-Q system and used throughout all the experiments.

### *2.2. Preparation of $Fe_3O_4$-$Ab_1$ conjugates*

The carboxylated $Fe_3O_4$ (100 nm) was decorated with $Ab_1$ through EDC/NHS chemistry. In the beginning, 400 μL of $Fe_3O_4$ (10 mg/mL) liquid dispersion was centrifuged to remove the solvent using a centrifuge (3000 rpm, 3 min). Subsequently, 400 μL of coupling buffer (0.1 mol/L PBS,

pH = 6.0) was dropped into that centrifuge tube. The above steps were repeated 3 times to ensure the $Fe_3O_4$ was completely redispersed in the coupling buffer. Next, 40 μL of EDC (50 mg/mL) and 40 μL of NHS (50 mg/mL) were added to the tube, the mixture was then incubated in an oscillator at room temperature for 20 min. After the carboxyl groups on the surfaces of $Fe_3O_4$ were fully activated, a centrifuge (3000 rpm, 3 min) was used again to remove the unreacted EDC and NHS. The sediment after centrifugation was redispersed in 400 μL of coupling buffer for the connection of $Ab_1$. Then, 20 μL of $Ab_1$ (1 mg/mL) was added to the mixture, followed by incubation in a shaker at room temperature for 2 h to achieve a valid coupling between $Fe_3O_4$ and $Ab_1$. For the removal of unbound $Ab_1$, the mixture was centrifuged at 3000 rpm for 3 min. The obtained sediment was then resuspended in 400 μL of blocking buffer (20 mmol/L Tris, pH = 8.0) and incubated at room temperature for 1 h to block the residual activated carboxyl groups. At last, the mixture was centrifuged and redispersed in 400 μL of storage buffer (0.1 mol/L, pH = 7.4) containing 0.01% of Tween® 20 and 0.1 % of BSA.

*2.3. Preparation of GPG-$Ab_2$ probe*

The $Gd^{3+}$ loaded $PEG_6$ modified GQDs (GPG) were prepared following the previously proposed method. Briefly, 15 mg of GQDs and 0.05 mmol of $PEG_6$ were dissolved in 15 mL of deionized water and then transferred into autoclave heating at 240 ℃ for 48 h. After the mixture cooled down naturally, $Gd(NO_3)_3$•$6H_2O$ (225.7 μg, 0.5 μmol) was added to it and then heated for another 24 h at 240 ℃. Next, the obtained solution was dialyzed in a 3500 Da dialysis bag against deionized water to remove the dissociative $Gd^{3+}$. At last, GPG powder was obtained by a lyophilizer.

To prepare the GPG-$Ab_2$ probe, GPG was first activated to be able to bind $Ab_2$. Similar to the preparation of $Fe_3O_4$-$Ab_1$, 15 mg of GPG powder was dissolved in 1 mL of coupling buffer (0.1 mol/L PBS, pH = 6.0). Next, 100 μL of EDC (50 mg/mL) and 100 μL of NHS (50 mg/mL) were

dropped into the GPG solution in order, the mixture was then incubated in a shaker at room temperature for 20 min to activate the carboxyl groups on the surface of GPG. After that, $Ab_2$ (500 μL, 1 mg/mL) was added to the mixture, which was shaken at room temperature for 2 h to connect the GPG. The obtained mixture was placed in the ultrafiltration centrifuge tube (3000 Da, 9000 rpm, 10 min) to remove the unbound $Ab_2$ and unreacted EDC/NHS. Next, the filtered mixture was redispersed in 1 mL of blocking buffer (20 mmol/L Tris, pH = 8.0) and incubated at room temperature for 1 h to block the residual activated carboxyl groups. At last, the mixture was treated by ultrafiltration centrifugation (3000 Da, 9000 rpm, 10 min) and resuspended in 1 mL of storage buffer (0.1 mol/L, pH = 7.4) containing 0.01% of Tween® 20 and 0.1 % of BSA. The above usage can be scaled up to obtain a large number of probes.

### *2.4. Collection and pretreatment of human serum*

Human whole blood samples of 14 human participants were initially collected in anticoagulant tubes and stored at 4 ℃. Each human serum sample was separated from the human blood using a centrifuge (3200 rpm, 3 min) and then diluted with PBS buffer (pH = 7.2) before use. The studies involving human participants were reviewed and approved by The Ethical Committee of Huashan Hospital. Human participants provided their informed consent.

## 3. Results and discussion

### *3.1. Strategy of the MRS assays*

As illustrated in **Scheme 1**, the MS-MRS assay can be divided into 5 steps. In the first step, the magnetic carrier ($Fe_3O_4$-$Ab_1$), magnetic probe (GPG-$Ab_2$) containing GQDs and $Gd^{3+}$, and the samples containing CD105 are mixed and incubated. Both the magnetic carrier and magnetic probe can bind with CD105 through antigen-antibody reaction but *via* the different binding sites of

CD105. Next, the mixture is treated by a magnet outside the sample vial to separate the magnetic carriers and biomolecules bound to the carriers from the incubated mixture. Some of the magnetic probes will also be separated because of the indirect binding with the magnetic carrier (*i.e.*, the magnetic carrier and magnetic probe are bound together to CD105). Thirdly, the supernate of the mixture is collected. Fourthly, the ULF NMR relaxometry is used to measure the $T_1$ of supernate. Finally, by calculating the difference of $T_1$ values of the test samples and the control samples, the amount of CD105 can be derived using the calibration curve. For the G-MRS without magnetic separation (**Scheme S1**), after the incubation of the test samples and the magnetic probes, the mixture can be directly used for $T_1$ measurement.

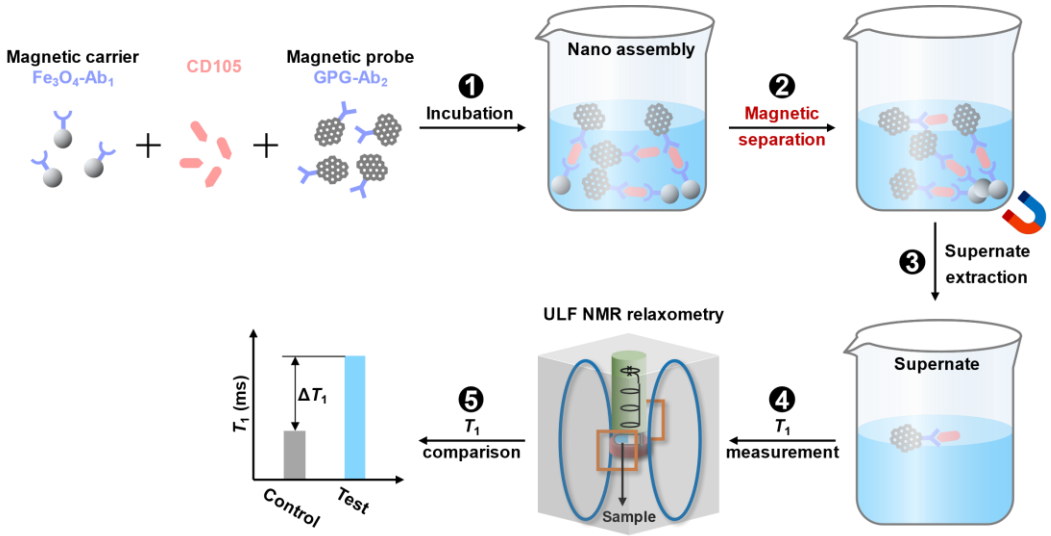


**Scheme 1.** Illustration of MS-MRS assay.

*3.2. Magnetic separation efficiency of $Fe_3O_4$*

Before the preparation of $Fe_3O_4$-$Ab_1$ conjugates, the optimal size of $Fe_3O_4$ and magnetic separation time were investigated. The transmission electron microscope (TEM) image (**Fig. 1A**) and scanning electron microscope (SEM) image (**Fig. 1B)** correspond to the morphologies of carboxylated $Fe_3O_4$ with different diameters, both the two kinds of carboxylated $Fe_3O_4$ show high

uniformity in size. The size distribution histogram of carboxylated $Fe_3O_4$ (labeled as 50 nm) related to **Fig. 1A** was plotted in **Fig. S1**. The average diameter was found to be 50.8 ± 0.9 nm. The statistical diameter of the other carboxylated $Fe_3O_4$ (labeled as 100 nm) was fitted as 136.1 ± 3.0 nm (**Fig. S2**). To balance the dispersity in water and the magnetic separation efficiency, these carboxylated $Fe_3O_4$ nanoparticles with different diameters (50.8 and 136.1 nm) were chosen as the candidates to form magnetic carriers in the MS-MRS assay.

Next, the transverse relaxation rates ($1/T_2$) of those carboxylated $Fe_3O_4$ with different concentrations were measured with ULF NMR relaxometry by dispersing them in 10 mL of deionized water. As depicted in **Fig. 1C**, linear fits of $1/T_2$ *vs*. concentration of carboxylated $Fe_3O_4$ were employed to determine the transverse relaxivities ($r_2$) values. The $r_2$ values are 6278.7 ± 498.6 and 206.8 ± 14.9 L/(mg·s) of carboxylated $Fe_3O_4$ with the diameters of 50.8 and 136.1 nm, respectively ($R^2 > 0.98$). Since the carboxylated $Fe_3O_4$ particles are designed to capture instead of signaling the biomarkers, their relaxivities are insignificant for the choice of the proper size to form the $Fe_3O_4$-$Ab_1$ conjugates. The $r_2$ values can be regarded as the reference for determining the carboxylated $Fe_3O_4$ concentrations in the following magnetic separation efficiency studies.

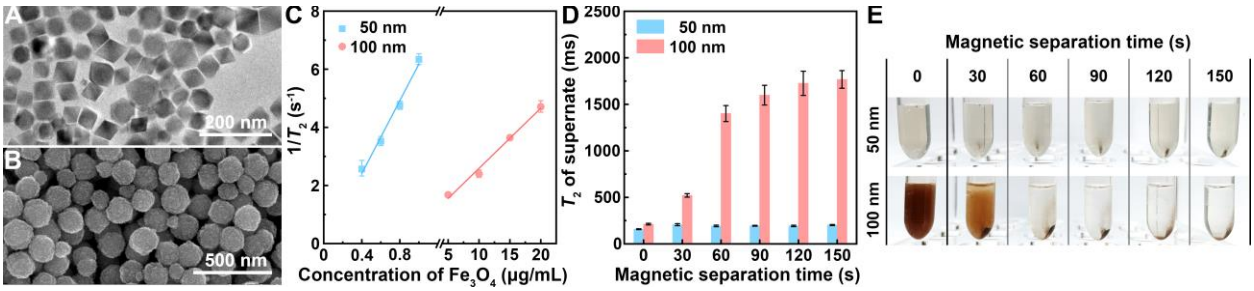


**Fig. 1.** Characterizations of carboxylated $Fe_3O_4$. (A) TEM image of $Fe_3O_4$ with the size of 50 nm. (B) SEM image of $Fe_3O_4$ with the size of 100 nm. (C) The $r_2$ fittings of $Fe_3O_4$ with different sizes. The comparisons of (D) supernatant $T_2$ values and (E) photographs when the aqueous dispersions of $Fe_3O_4$ were treated by a magnet at different times. Error bars indicate errors in the fitting.

Before the magnetic separation process, the concentrations of the carboxylated $Fe_3O_4$ are 1 and 20 μg/mL when the diameters are 50 and 100 nm, respectively. **Fig. 1D** compares the $T_2$ values of

supernate acquired after magnetic separation at different times. Without the treatment of the magnet, the $T_2$ values of carboxylated $Fe_3O_4$ (50 nm) and $Fe_3O_4$ (100 nm) are 157.7 ± 4.6 and 212.3 ± 9.0 ms, respectively. With the increase of magnetic separation time, the $T_2$ value of carboxylated $Fe_3O_4$ (100 nm) keeps increasing to 1725.8 ± 130.0 ms in the first 120 s and reaches the value similar to the $T_2$ of $H_2O$ (**Fig. S3**) measured under the same circumstances, meaning the magnetic separation of carboxylated $Fe_3O_4$ (100 nm) is sufficient. Oppositely, the supernate of carboxylated $Fe_3O_4$ (50 nm) shows no remarkable changes in the $T_2$ value. The photographs in **Fig. 1E** visually support the above results that carboxylated $Fe_3O_4$ (100 nm) can be easily separated by a magnet in a short time (120 s), in which the concentrations of carboxylated $Fe_3O_4$ (50 nm) and $Fe_3O_4$ (100 nm) are 20 and 400 μg/mL, respectively. The above results enable carboxylated $Fe_3O_4$ (100 nm) as the magnetic carrier in the MS-MRS assay.

### *3.3. Characterizations of GPG*

The morphological characterizations of GPG are displayed in **Fig. 2A** and **B**. In the TEM image of GPG (**Fig. 2A**), the evenly-distributed state results from the highly dispersed GPG in water. By measuring the diameters of the GPG particles, the average diameter was fitted to be 6.6 ± 0.2 nm (**Fig. S4**) by using the Gaussian distribution function. In the high-resolution TEM (HR-TEM) image of GPG (**Fig. 2B**), an unambiguous honeycomb structure of graphene can be observed, indicating that GPG has the graphene structure.

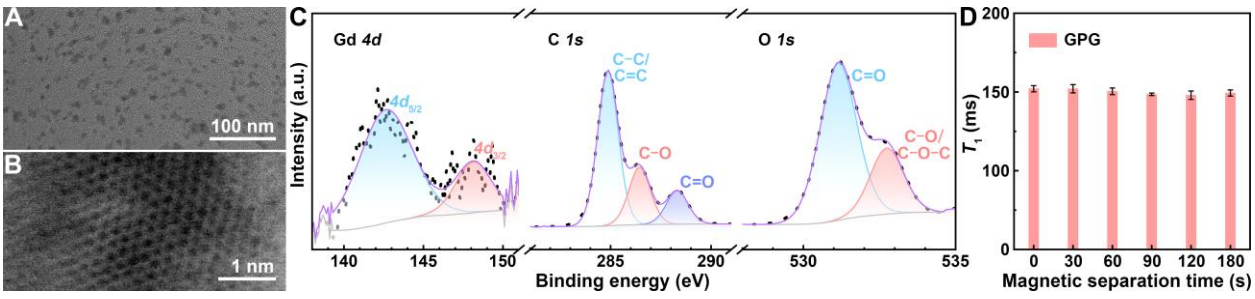

**Fig. 2.** Characterizations of GPG. (A) TEM and (B) HR-TEM images of GPG. (C) The XPS Gd *4d*, C *1s*, and O *1s* spectra of GPG. (D) $T_1$ comparison of GPG after different treating times of magnetic separation. Error bars indicate errors in the fitting.

The chemical structure of GPG was investigated by X-ray photoelectron spectroscopy (XPS). The atomic ratio of C to O is 2.2, indicating that GPG has abundant oxygen-containing groups. As shown in **Fig. 2C**, two peaks located at 142.6 and 148.1 eV are the signals of Gd $4d_{5/2}$ and $4d_{3/2}$ in the Gd *4d* spectrum [25], meaning that the $Gd^{3+}$ was bound with $PEG_6$ in GPG. The C *1s* spectrum delivers a piece of important information that the oxygen-containing groups take a large proportion (38.3%) of the GPG. In that spectrum, peaks at 284.9, 286.4, and 288.3 eV represent C–C/C=C, C–O, and C=O bonds [32], the latter two bonds evidencing the presence of carboxyl. As shown in the O *1s* spectrum, two peaks located at 531.1 and 532.7 eV can be recognized as C=O and C–O/C–O–C bonds [33], verifying the abundance of carboxyl groups.

GPG holds a high longitudinal relaxivity ($r_1$) of 90.9 L $mmol^{-1}$ $s^{-1}$ (**Fig. S5**), such a high value ensures a sensitive detection of biomarkers when forming a magnetic probe. As GPG will be used to connect $Ab_2$ and serve as the magnetic probe, it should not be separated by a magnet or other magnetic fields. GPG was dispersed in deionized water at the $Gd^{3+}$ concentration of 0.05 mmol/L for magnetic separation. As shown in **Fig. 2D**, when the mixture was untreated with the magnet (time = 0), GPG has a $T_1$ of 204.1 ± 3.9 ms. With the increase in separation time, the $T_1$ value remains unchanged, indicating that GPG cannot be magnetically separated.

*3.4. Monitoring of the binding processes in assays with ULF NMR relaxometry*

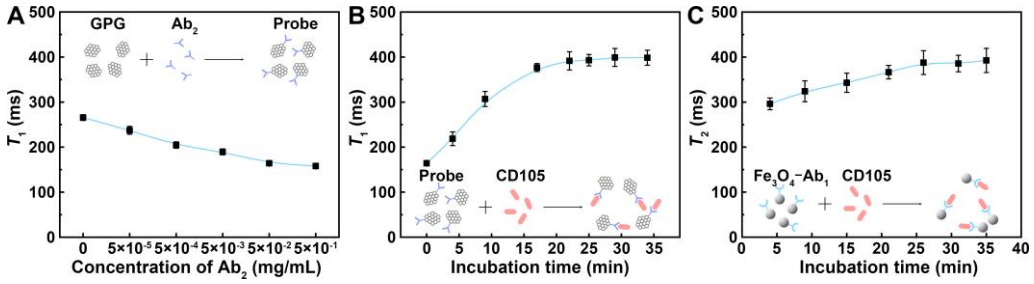

**Fig. 3.** Optimizations of the assays. (A) $T_1$ comparison of GPG-$Ab_2$ (Probe) with different $Ab_2$ amounts. (Inset: depiction of the binding between GPG and $Ab_2$) (B) $T_1$ changes *vs*. time when the probe was incubated with CD105 (Inset: depiction of CD105 detection with the probe). (C) $T_2$ changes *vs*. time when $Fe_3O_4$-$Ab_1$ was incubated with CD105 (Inset: depiction of CD105 detection with the $Fe_3O_4$-$Ab_1$). Error bars indicate errors in the fitting.

Before carrying out the MS-MRS assay, the magnetic probe should be optimized to make full use of the GPG and possess a high sensitivity, the binding amount of $Ab_2$ was thus optimized by measuring the $T_1$ of the probe with ULF NMR relaxometry. Different concentrations (0, 0.001, 0.01, 0.1, 1, and 10 mg/mL) of $Ab_2$ were added when preparing the GPG-$Ab_2$ probe (see 2.3. Preparation of GPG-$Ab_2$ probe). As recorded in **Fig. 3A**, the $T_1$ decreases when the binding amount of $Ab_2$ increases and then settles at around 160.0 ms when the concentration of $Ab_2$ is 0.05 mg/mL (corresponding to the adding concentration of 1 mg/mL). In **Fig. 3A**, the abscissa represents the concentration of $Ab_2$ that was diluted 20 times (sample volume is 10 mL), and the concentration of $Gd^{3+}$ in GPG is 0.05 mmol/L. Therefore, the probe follows a ratio (1 mmol : 1 g) of $Gd^{3+}$ to $Ab_2$.

The incubation time largely determines the time consumption of the MRS assay. To investigate the optimal incubation time of MS-MRS assay, the magnetic carrier ($Fe_3O_4$-$Ab_1$) and magnetic probe (GPG-$Ab_2$) are used to bind the CD105, and ULF NMR relaxometry is used to monitor the incubation in real time by measuring the $T_1$ of the mixture. During the incubation, the relaxation time ($T_1$ or $T_2$) was measured every 5 min. As displayed in **Fig. 3B**, the probe with a $Gd^{3+}$ concentration of 0.05 mmol/L was used to detect CD105 (50 μg/mL). $T_1$ at 0 min represents the $T_1$ value of the control sample. **Fig. 3B** reveals that with the increase in incubation time, the $T_1$ value of the mixture rises in the first 22 min and then stabilizes at 390 ms, which reveals that the binding between GPG-$Ab_2$ and CD105 terminates in 22 min. Analogously, the binding between $Fe_3O_4$-$Ab_1$ (20 μg/mL) and CD105 (50 μg/mL) finishes in 26 min with almost an unchanged $T_2$ value of 385 ms (**Fig. 3C**). Therefore, the optimal incubation time for MS-MRS is the maximum of the two

times, *i.e.*, 26 min. In addition, when detecting the CD105 with the same concentration, GPG-$Ab_2$ shows a larger change in relaxation time compared with that involving $Fe_3O_4$-$Ab_1$, indicating the probe can be prospectively used to develop a sensitive MRS without magnetic separation.

*3.5. Sensitive and quantitative detection of CD105 in PBS buffer*

Using the above-mentioned optimal settings, MRS assays without and with magnetic separation were developed with high specificity (**Fig. S6**). Different concentrations (0, 0.5 ng/mL, 5 ng/mL, 50 ng/mL, 0.5 μg/mL, 5 μg/mL, and 50 μg/mL) of CD105 liquid dispersion (PBS buffer, pH = 7.2) were used to find the limit of detection (LOD) of G-MRS. As displayed in **Fig. 4A**, the control sample has a $T_1$ of 166.8 ± 7.0 ms with the $Gd^{3+}$ concentration of 0.05 mmol/L. With the addition of CD105, $T_1$ goes up gradually. $T_1$ values measured by ULF NMR relaxometry are 167.2 ± 1.9, 174.6 ± 2.8, 195.9 ± 8.4, 264.9 ± 9.0, 354.1 ± 19.1, 406.8 ± 26.8 ms when the concentrations of CD105 are 0.5 ng/mL, 5 ng/mL, 50 ng/mL, 0.5 μg/mL, 5 μg/mL, and 50 μg/mL, respectively. The significance levels marked in **Fig. 4A** indicate that when the concentrations of CD105 are 0.5 and 5 ng/mL, $T_1$ values have no significance compared with that of the control sample. With concentrations larger than 5 ng/mL, $T_1$ values show significance compared with that of the control sample. Ulteriorly, a linear relationship between $\Delta T_1$ (difference between $T_1$ values of the test sample and the control sample) values and CD105 concentrations can be found in the concentration range from 50 ng/mL to 50 μg/mL. As plotted in **Fig. 4B**, the fitting line can be described as $y = 73.1\ x - 96.1$ ($R^2 = 0.99371$) when the $x$-axis represents the logarithm of CD105 concentration. The LOD can be then determined from the curve when $\Delta T_1$ equals the $\Delta T_1$ of the control sample plus 3 times the standard deviation (21.0 ms) and corresponds to 40.0 ng/mL [34]. The limit of quantitation (LOQ) can be evaluated from the curve when $T_1$ equals the $T_1$ of the control sample plus 10 times the SD (70.0 ms) and corresponds to 187.2 ng/mL [35].

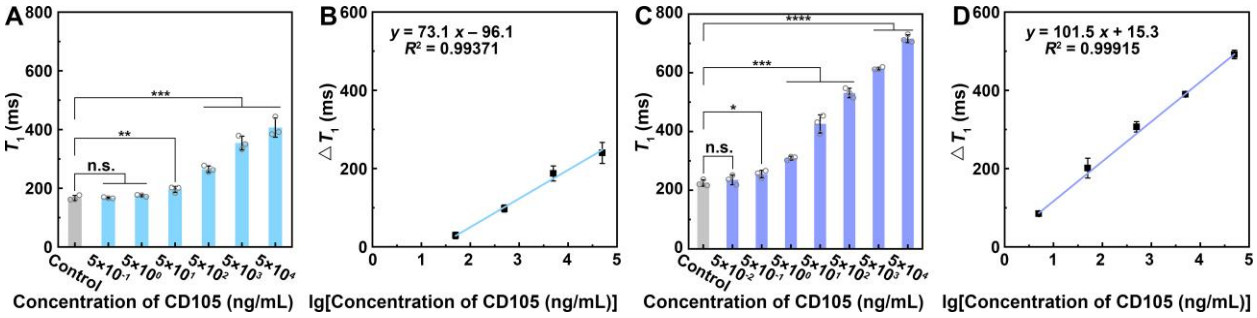


**Fig. 4.** Sensitive and quantitative detection of CD105 in PBS buffer. (A) $T_1$ values measured with different concentrations of CD105 in the G-MRS assay. (B) A linear relationship between $\Delta T_1$ values and the logarithm of CD105 concentrations in the G-MRS assay. (C) $T_1$ values measured with different concentrations of CD105 in the MS-MRS assay. (D) A linear relationship between $\Delta T_1$ values and the logarithm of CD105 concentrations in MS-MRS assay. Error bars indicate the standard deviation (SD) of three replicates of different samples executing the entire assay. Significance levels analyzed by Two-tail Student's T-test are shown as: n.s., no significance, $P > 0.05$; $^{*}P < 0.05$; $^{**}P < 0.01$; $^{***}P < 0.001$; $^{****}P < 0.0001$.

In **Fig. 4C**, an additional concentration (50 pg/mL) of CD105 was used to determine the LOD of MS-MRS. The concentration of $Fe_3O_4$ in the magnetic carrier is 20 μg/mL, and the $Gd^{3+}$ concentration in the magnetic probe is 0.05 mmol/L. The $T_1$ values are 224.4 ± 9.0, 235.0 ± 13.5, 254.8 ± 10.3, 309.2 ± 5.4, 425.8 ± 25.3, 531.1 ± 13.3, 614.4 ± 3.6, 715.9 ± 10.9 when the concentrations of CD105 in PBS buffer (pH = 7.2) are 0 (control), 50 pg/mL, 0.5 ng/mL, 5 ng/mL, 50 ng/mL, 0.5 μg/mL, 5 μg/mL, and 50 μg/mL, respectively. When the CD105 concentration exceeds 50 pg/mL, $T_1$ values significantly differ from that of the control sample. The linear region of MS-MRS is also wider than that of G-MRS, *i.e.*, from 5 ng/mL to 50 μg/mL. As shown in **Fig. 4D**, the linear relationship between $\Delta T_1$ and the logarithm of CD105 concentration can be fitted as $y = 101.5\,x + 15.3$ with $R^2 = 0.99915$. The LOD of MS-MRS for CD105 detection is thus estimated to be 1.3 ng/mL, which is sensitive than that of G-MRS (40.0 ng/mL). Additionally, the LOQ is determined as 5.4 ng/mL. The above relationship can be used to quantitively analyze the concentration of CD105 in real samples. Although the reported methods for CD105 detection show high sensitivity compared to that of MS-MRS (**Table S1**), the linear region of MS-MRS is wider

than those methods. Such a broad detection region can be used to quickly determine the CD105 concentrations without reduplicative dilution of samples. Meanwhile, MS-MRS can be applied in the fast detection of CD105 within 30 min (26 min for sample incubation and 2 min for $T_1$ measurement).

Based on the above results, the MS-MRS assay is superior in performance compared with G-MRS: i) Better sensitivity. MS-MRS has a LOD of 1.3 ng/mL, which is more sensitive than G-MRS (25.0 ng/mL). ii) Remarkable linear region. MS-MRS possesses a linear region that spans 5 orders of magnitude, which is beneficial for the quantitative determination of CD105. iii) More distinguishable $T_1$ values. When detecting the same concentration of CD105, $T_1$ of MS-MRS usually shows a smaller *P*-value (more significant difference) compared with that of G-MRS. This will help to realize precise detection with a wide dynamic range.

*3.6. Quantitative detection of CD105 in human serum*

The ability of quantitative CD105 detection in the real sample was evaluated by detecting CD105 in human serum. Before executing the MS-MRS assay, human serum was diluted with PBS buffer (pH = 7.2) to weaken the background and ensure the specificity of the probe. As shown in **Fig. S7**, the $T_1$ value of diluted human serum increases and approaches the $T_1$ of PBS buffer with increasing diluted times. When the human serum was diluted with PBS buffer 50 times, the $T_1$ of the diluted human serum shows no significance with that of PBS buffer, suggesting that the human serum should be diluted 50 times in the MS-MRS assay.

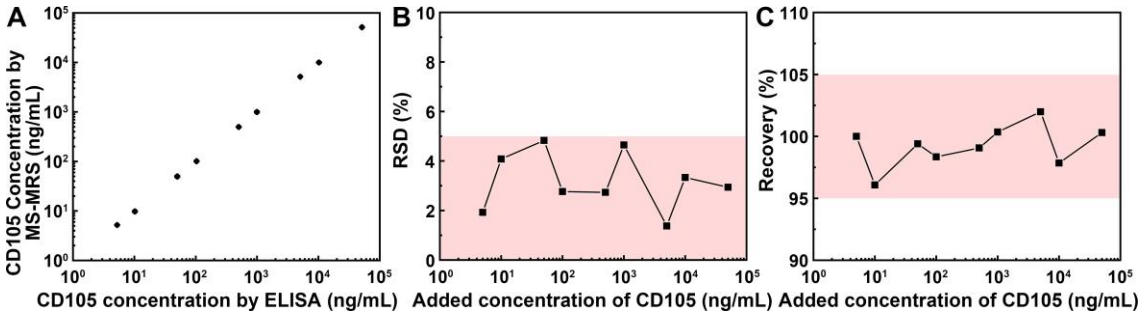


**Fig. 5.** Quantitative detection of CD105 in human serum. (A) The concentration of CD105 measured by MS-MRS versus the concentration of CD105 measured by ELISA in diluted human serum. Error bars indicate the SD of three replicates of different samples (CD105 dispersed in diluted human serum from different human participants) executing the entire assay. (B) RSD of MS-MRS assay for CD105 detection in diluted human serum. (C) Recovery of MS-MRS assay for CD105 detection in diluted human serum.

To investigate the performance of MS-MRS in quantitative CD105 detection, 9 groups of human serum samples were prepared containing different concentrations of CD105 ranging from 0 to 50 μg/mL (**Table S2**). In each group, CD105 with the same amount was individually dispersed in diluted human serum samples collected from 3 participants. In the group of control samples, no CD105 was added to the diluted human serum. The measured $T_1$ of the control sample is 258.0 ± 9.0 ms, which can be served as a minuend in the following experiments to calculate the $\Delta T_1$ values and CD105 concentrations. Next, CD105 with different concentrations (5 ng/mL, 10 ng/mL, 50 ng/mL, 0.1 μg/mL, 0.5 μg/mL, 1 μg/mL, 5 μg/mL, 10 μg/mL, and 50 μg/mL) were spiked into the diluted human serum from different human participants, respectively. The $\Delta T_1$ values of the above samples are listed in **Table S2**. As depicted in **Fig. 5A**, the CD105 concentrations determined by MS-MRS assay linearly correlated with those measured by ELISA assay. To evaluate the quantitative performance, the relative SD (RSD) and recovery are introduced. The RSD values of the MS-MRS assay are less than 5% (**Fig. 5B**, **Table S2**), which proves that the assay has high consistency in CD105 detection in a wide range of concentrations. The recovery of MS-MRS varies from 96.1% to 102.0% in the linear region from 5 ng/mL to 50 μg/mL (**Fig. 5C**, **Table S2**), indicating that the proposed assay has good accuracy.

High accuracy and consistency have been achieved for CD105 detection using the MS-MRS assay. Nevertheless, according to the linear relationship in **Fig. 4D**, a small change (a few milliseconds) in $\Delta T_1$ values leads to a large change in the found CD105 concentrations, which makes the improvement in the accuracy and consistency of the assay challenging. Therefore, more attention should be paid to improving the accuracy of $T_1$ acquisition in ULF NMR relaxometry.

## 4. Conclusions

To conclude, by combining $Fe_3O_4$ as the magnetic carrier and GPG as the magnetic label, the magnetic separation integrated with ULF NMR relaxometry was developed for CD105 detection. After connecting different antibodies against CD105 with $Fe_3O_4$ and GPG, separately, both the magnetic carrier and magnetic label can be used to bind CD105. Compared with G-MRS, magnetic separation-assisted MRS shows a sensitive LOD as low as 1.3 ng/mL, a remarkably wide linear region from 5 ng/mL to 50 μg/mL, and more distinguishable $T_1$ values. The low RSD (<5%) and recovery (96.1–102.0%) show that MS-MRS can be applied in CD105 detection in real human serum samples with high accuracy and consistency. This newly developed MS-MRS assay with impressive performances can not only be applied in the detection of other biomolecules by changing the antibodies, but can also be used in the NMR relaxometry working at higher magnetic fields.

## Declaration of competing interest

The authors declare that they have no known competing financial interests or personal relationships that could have appeared to influence the work reported in this paper.

## CRediT authorship contribution statement

**Yongqiang Li:** Conceptualization, Methodology, Writing - Original Draft; **Zhifeng Shi:** Conceptualization, Methodology, Validation; **Liuyang Shang:** Investigation, Validation, Writing

- Original Draft; **Quan Tao:** Resources, Software; **Qisheng Tang:** Methodology, Validation; **Hans-Joachim Krause:** Writing - Review & Editing, Funding acquisition; **Siwei Yang:** Writing - Review & Editing, Funding acquisition; **Guqiao Ding:** Supervision; **Hui Dong:** Writing - Review & Editing, Funding acquisition, Supervision; **Xiaoming Xie:** Supervision.

**Acknowledgments**

Y.Q. Li and Z.F. Shi contributed equally to this work. This work was financially supported by the National Natural Science Foundation of China (11874378), Science and Technology Commission of Shanghai Municipality (21ZR1482800, 21S31903200), Shanghai Municipal Science and Technology Major Project (2018SHZDZX01), and Mobility Programme of the Sino-German Center for Research Promotion (M-0022).

**Appendix A. Supplementary data**

Supplementary data to this article can be found online at https://doi.org/10.1016/j.snb.

**References**

[1] P. Gillis, F. Moiny, R.A. Brooks, On $T_2$-shortening by strongly magnetized spheres: A partial refocusing model, Magn. Reson. Med., 47 (2002) 257–263.
[2] C. Min, H.L. Shao, M. Liong, T.J. Yoon, R. Weissleder, H. Lee, Mechanism of magnetic relaxation switching sensing, ACS Nano, 6 (2012) 6821–6828.
[3] K. Wu, R. Saha, D.Q. Su, V.D. Krishna, J.M. Liu, M.C.J. Cheeran, et al., Magnetic-nanosensor-based virus and pathogen detection strategies before and during COVID-19, ACS Appl. Nano Mater., 3 (2020) 9560–9580.
[4] X.Q. You, D.C. Zhang, K.W. Yao, Y.Q. Huang, M. Liu, J.Y. Xie, et al., Ultrasensitive and fast detection of pathogens using Europium-containing polystyrene nanospheres in a homemade portable NMR diagnostic system, Sens. Actuators B Chem., 320 (2020) 128370.
[5] S. Bamrungsap, M.I. Shukoor, T. Chen, K. Sefah, W.H. Tan, Detection of lysozyme magnetic relaxation switches based on aptamer-functionalized superparamagnetic nanoparticles, Anal. Chem., 83 (2011) 7795–7799.
[6] Y.B. Ling, T. Pong, C.C. Vassiliou, P.L. Huang, M.J. Cima, Implantable magnetic relaxation sensors measure cumulative exposure to cardiac biomarkers, Nat. Biotechnol., 29 (2011) 273–277.
[7] W. Wang, P.X. Ma, H. Dong, H.J. Krause, Y. Zhang, D. Willbold, et al., A magnetic nanoparticles relaxation sensor for protein-protein interaction detection at ultra-low magnetic field, Biosens. Bioelectron., 80 (2016) 661–665.
[8] Y.T. Chen, R. Medhi, I. Nekrashevich, D. Litvinov, S.J. Xu, T.R. Lee, Specific detection of proteins using exceptionally responsive magnetic particles, Anal. Chem., 90 (2018) 6749–6756.

[9] S. Bamrungsap, T. Chen, M.I. Shukoor, Z. Chen, K. Sefah, Y. Chen, et al., Pattern recognition of cancer cells using aptamer-conjugated magnetic nanoparticles, ACS Nano, 6 (2012) 3974–3981.
[10] A.A. Ghazani, C.M. Castro, R. Gorbatov, H. Lee, R. Weissleder, Sensitive and direct detection of circulating tumor cells by multimarker micro-nuclear magnetic resonance, Neoplasia, 14 (2012) 388–395.
[11] C.M. Castro, A.A. Ghazani, J. Chung, H.L. Shao, D. Issadore, T.J. Yoon, et al., Miniaturized nuclear magnetic resonance platform for detection and profiling of circulating tumor cells, Lab Chip, 14 (2014) 14–23.
[12] H.J. Chung, C.M. Castro, H. Im, H. Lee, R. Weissleder, A magneto-DNA nanoparticle system for rapid detection and phenotyping of bacteria, Nat. Nanotechnol., 8 (2013) 369–375.
[13] Y. Zhao, Y.X. Li, K. Jiang, J. Wang, W.L. White, S.P. Yang, et al., Rapid detection of *Listeria monocytogenes* in food by biofunctionalized magnetic nanoparticle based on nuclear magnetic resonance, Food Control, 71 (2017) 110–116.
[14] X. Wang, S.P. Ni, Y.N. Wang, An aptamer-functionalized magnetic relaxation switch sensor for the rapid detection of vibrio alginolyticus in water, Appl. Magn. Reson., 52 (2021) 1561–1580.
[15] H. Xing, C.L. Zhang, G. Ruan, J.J. Zhang, K. Hwang, Y. Liu, Multimodal detection of a small molecule target using stimuli-responsive liposome triggered by aptamer-enzyme conjugate, Anal. Chem., 88 (2016) 1506–1510.
[16] L. Gloag, M. Mehdipour, D.F. Chen, R.D. Tilley, J.J. Gooding, Advances in the application of magnetic nanoparticles for sensing, Adv. Mater., 31 (2019) 1904385.
[17] Z.C. Xu, C. Liu, S.J. Zhao, S. Chen, Y.C. Zhao, Molecular sensors for NMR-based detection, Chem. Rev., 119 (2019) 195–230.
[18] Y. Dong, C.-y. Wen, Y. She, Y. Zhang, Y. Chen, J. Zeng, Magnetic relaxation switching immunoassay based on hydrogen peroxide-mediated assembly of Ag@Au–$Fe_3O_4$ nanoprobe for detection of aflatoxin b1, Small, 17 (2021) 2104596.
[19] X.Y. Xu, R. Ray, Y.L. Gu, H.J. Ploehn, L. Gearheart, K. Raker, et al., Electrophoretic analysis and purification of fluorescent single-walled carbon nanotube fragments, J. Am. Chem. Soc., 126 (2004) 12736–12737.
[20] A.L. Xu, G. Wang, Y.Q. Li, H. Dong, S.W. Yang, P. He, et al., Carbon-based quantum dots with solid-state photoluminescent: Mechanism, implementation, and application, Small, 16 (2020) 2004621.
[21] J.P. Li, S.W. Yang, Y. Deng, P.W. Chai, Y.C. Yang, X.Y. He, et al., Emancipating target-functionalized carbon dots from autophagy vesicles for a novel visualized tumor therapy, Adv. Funct. Mater., 28 (2018) 1800881.
[22] A. Xu, P. He, C. Ye, Z. Liu, B. Gu, B. Gao, et al., Polarizing graphene quantum dots toward long-acting intracellular reactive oxygen species evaluation and tumor detection, ACS Appl. Mater. Interfaces, 12 (2020) 10781-10790.
[23] J.P. Li, S.W. Yang, Z.Y. Liu, G. Wang, P. He, W. Wei, et al., Imaging cellular aerobic glycolysis using carbon dots for early warning of tumorigenesis, Adv. Mater., 33 (2021) 2005096.
[24] Y.Q. Li, P.X. Ma, Q. Tao, H.-J. Krause, S.W. Yang, G.Q. Ding, et al., Magnetic graphene quantum dots facilitate closed-tube one-step detection of SARS-CoV-2 with ultra-low field NMR relaxometry, Sens. Actuators B Chem., 337 (2021) 129786.

[25] Y.Q. Li, H. Dong, Q. Tao, C.C. Ye, M.M. Yu, J.P. Li, et al., Enhancing the magnetic relaxivity of MRI contrast agents *via* the localized superacid microenvironment of graphene quantum dots, Biomaterials, 250 (2020) 120056.
[26] C. Kaittanis, S. Santra, J.M. Perez, Role of nanoparticle valency in the nondestructive magnetic-relaxation-mediated detection and magnetic isolation of cells in complex media, J. Am. Chem. Soc., 131 (2009) 12780–12791.
[27] I. Koh, R. Hong, R. Weissleder, L. Josephson, Nanoparticle-target interactions parallel antibody-protein interactions, Anal. Chem., 81 (2009) 3618–3622.
[28] Y.P. Chen, Y.L. Xianyu, Y. Wang, X.Q. Zhang, R.T. Cha, J.S. Sun, et al., One-step detection of pathogens and viruses: Combining magnetic relaxation switching and magnetic separation, ACS Nano, 9 (2015) 3184–3191.
[29] Y.L. Xianyu, Y.Z. Dong, Z. Zhang, Z.H. Wang, W.B. Yu, Z.L. Wang, et al., $Gd^{3+}$-nanoparticle-enhanced multivalent biosensing that combines magnetic relaxation switching and magnetic separation, Biosens. Bioelectron., 155 (2020) 112106.
[30] M.J.A. Schoonderwoerd, M.-J.T.H. Goumans, L.J.A.C. Hawinkels, Endoglin: Beyond the endothelium, Biomolecules, 10 (2020) 289.
[31] E. Fonsatti, H.J.M. Nicolay, M. Altomonte, A. Covre, M. Maio, Targeting cancer vasculature *via* endoglin/CD105: A novel antibody-based diagnostic and therapeutic strategy in solid tumours, Cardiovasc. Res., 86 (2010) 12–19.
[32] T.R. Gengenbach, G.H. Major, M.R. Linford, C.D. Easton, Practical guides for x-ray photoelectron spectroscopy (xps): Interpreting the carbon 1s spectrum, J. Vac. Sci. Technol., A, 39 (2021) 013204.
[33] P.G. Rouxhet, A.M. Misselyn-Bauduin, F. Ahimou, M.J. Genet, Y. Adriaensen, T. Desille, et al., Xps analysis of food products: Toward chemical functions and molecular compounds, Surf. Interface Anal., 40 (2008) 718–724.
[34] W.J. Lu, Y.P. Chen, Z. Liu, W.B. Tang, Q. Feng, J.S. Sun, et al., Quantitative detection of microrna in one step via next generation magnetic relaxation switch sensing, ACS Nano, 10 (2016) 6685–6692.
[35] A. Zuber, M. Purdey, E. Schartner, C. Forbes, B. van der Hoek, D. Giles, et al., Detection of gold nanoparticles with different sizes using absorption and fluorescence based method, Sens. Actuators B Chem., 227 (2016) 117–127.